Characterization of $K\alpha$ spectral profiles for vanadium, component redetermination for scandium, titanium, chromium, and manganese, and development of satellite structure for $Z=21$ to $Z=25$

C. T. Chantler, M. N. Kinnane, C.-H. Su, and J. A. Kimpton
School of Physics, University of Melbourne, Victoria 3010, Australia
(Received 30 August 2005; published 20 January 2006)

In most high-accuracy x-ray experiments, characteristic radiation is used to determine calibration energies or wavelengths. This paper presents experimental results for vanadium $K\alpha$, and component refitting for scandium, titanium, chromium, and manganese, addressing a critical limitation on the current use of this approach. The influence of spectrometer broadening upon the registration of these calibration profiles is quantitatively discussed and determined. The analysis permits such calibration with insignificant loss of accuracy compared to the reference uncertainty, down to a one part per million level. In the process we reveal key empirical structural trends in $K\alpha$ spectral profiles from $Z=21$ to $Z=25$ which originate from detailed physical processes which are neither well understood nor well evaluated theoretically.

DOI: 10.1103/PhysRevA.73.012508 PACS number(s): 32.30.Rj, 32.80.Hd, 31.30.Jv, 12.20.Fv

I. INTRODUCTION

In the x-ray regime, the link to the visible standard of the meter has been performed by x-ray and optical interferometry (XROI) of a high standard, by determining the lattice spacing of silicon [1–5]. A second link (the δ-d interferometer) transfers this standard to other lattice planes, other crystal samples, and highly regular crystals [6,7]. The link to current high-accuracy experiments is usually made by calibrating the energies of strong characteristic transitions ($K\alpha$ transitions in neutral solids, usually in elemental form), using a rigorously determined lattice spacing of a particular crystal. Limitations arise from the calibration accuracy of the particular $K\alpha$ standard, the consistency or robustness of the $K\alpha$ source, and the ability to measure or determine the profile to the same degree of precision. One may use different characteristic lines ($K\beta$ or L series, or absorption edges), but these calibration lines are normally less robustly determined.

In this paper we present experimental results for the $K\alpha$ profile of vanadium, and reevaluate profile characteristics for scandium, titanium, chromium, and manganese, to yield a complete series from $Z=21$ through $Z=25$. The use of component refitting on a consistent and uniform basis allows physical trends to inform theoretical predictions of characteristic and satellite structure in this region of energy and atomic number.

The latest and most comprehensive determination of theoretical characteristic transitions has been completed recently [8]. This study helps to confirm or question suspect measurements in a clear manner. The diagram lines (the primary contributions to the $K\alpha_1$ and $K\alpha_2$ peaks) are computed to a high degree of convergence, and in a consistent framework. This is a very valuable resource.

A few conventions must be explained. The "diagram line" for $K\alpha$ spectra is the $1s-2p$ transition energy with no excited spectator electrons. In response to the creation of a $1s$ hole in the K shell of the neutral element, a $2p$ L shell electron fills this hole. The $K\alpha$ spectrum therefore consists of two diagram lines corresponding to the energy separation of $2p_{3/2}$ and $2p_{1/2}$ levels. In experimental analysis, these two diagram lines are usually the dominant components of the spectral profile; and are usually labeled $K\alpha_{11}$ and $K\alpha_{21}$, assuming a unique and exact experimental interpretation. The spectrum also has satellite multiplets where an additional electron hole is created prior to decay (usually in the same process of electron bombardment which created the $1s$ hole). These multiplet spectra are dominated by transitions involving $1s3d$-$2l3d$ and $1s3p$-$2l3p$. Experimentally, additional (semi-empirical) components are fitted, labeled as $K\alpha_{1j}$ for satellites to the $K\alpha_{11}$ peak and $K\alpha_{2k}$ for satellites to the $K\alpha_{21}$ peak. The key to the current transfer of accuracy is that the compilations of references ([8] and earlier) link the energies of the peak locations of the experimental spectrum, which are labeled $K\alpha_1^0$ and $K\alpha_2^0$, to the eV and wavelength scales.

The theoretical problem of computing high-accuracy many-body perturbation theory (MBPT) computations (or other approaches) for neutral atoms, K resonant transition energies, and corresponding satellite and shake up resonances remains a formidable and generally unsolved problem. Diagram lines have been computed well, but satellite structure leads to asymmetric unresolved transition arrays (UTA's) which are difficult to calibrate or normalize. There has been some evidence for a key contribution of the asymmetry from $3p$ hole and $3d$ hole spectator satellite multiplets, but other mechanisms in the few studies attempting to do this have generally been discrepant from one another in the detailed multiplets and component amplitudes [9–12]. Recent work has also shown that this satellite structure is not constant but depends upon the exciting voltage or the excitation energy [13].

The theoretical (atomic or solid state) studies may be used as a guide, but the rigorous link for energy determination must be provided experimentally. The experimental determinations of characteristic resonances therefore determine our energy scale in most experiments.

Numerous independent studies of $K\alpha_{1,2}$ x-ray emission spectra of Sc [11], Ti [14], and 3*d* transition metals [12,15] were made over the past decade to serve the interests in fields such as atomic, plasma, and solid state physics. Asymmetric x-ray emisson spectra resulting from the simultaneous multielectronic transitions, observed as satellite peaks [16], were extensively discussed to be attributed to several equally probable mechanisms. As described by these earlier studies, analytic forms such as sums of Lorentzians and Voigts, introduced by Deutsch *et al.* [12] were employed to fit measured profiles remarkably well, so that the set of spectra now provides a basis for testing theoretical predictions concerning the atomic structures.

These results have been collected, edited, and compiled in a major summary [8]. The listing of locations of dominant ($K\alpha_1^0$ and $K\alpha_2^0$) peak energies is crucial for the calibration procedure outlined. However, for any real spectral profile to be used to calibrate the subsequent high-accuracy experiment, the asymmetry and satellite structure must also be known and defined, because to ignore the asymmetry is to shift the determined centroid or peak of the resulting fitted profile.

The experimental studies just mentioned allow a reconstruction of the profile from the sum of Voigt or Lorentzian peaks, which empirically must be the same for subsequent experiments using the same source. However, the crystal and detection system used is usually different, and usually of lower resolution, so that there is additional instrumental broadening (if nothing else). To attempt to fit a broadened profile with seven Voigt profiles with independent width parameters is usually impossible. Results typically just reveal the highly correlated parameter space used in the fitting procedure.

This parametrization difficulty is also displayed in the spread of fitting parameters between the different high-accuracy experimental $K\alpha$ calibrations, especially for the weakest peak components and their width parameters.

Of course the real transitions have several multiplets with complex structure and many components, so the modeling which has been performed using six or seven Lorentzian peak or Voigt peak profiles will only ever be an approximation to the physical reality. The inconsistency between the results, possible deconvolution procedures employed prior to fitting, and the choice of fitting profile prevents empirical trends, consistencies, and discrepancies in the physics of the transitional arrays from being observable.

In light of this, we have investigated a series of characteristic transitions suitable for calibrating a silicon or germanium crystal or other spectrometer system around a central energy of 5 keV, and determined a consistent calibration set which can be used for arbitrary experimental conditions of high or low accuracy and for high or low resolution. This has involved acquiring accurate analytic representation for each emission line profile, which can be described by a well-defined parametrization, as an essential component of a rigorously tied calibration procedure for any subsequent experiment. In the current situation, this has proceeded for the $K\alpha$ spectra of scandium ($Z=21$, 4 keV), titanium ($Z=22$, 4.5 keV), vanadium ($Z=23$, 5 keV), chromium ($Z=24$, 5.4 keV), and manganese ($Z=25$, 5.9 keV).

This 3*d* transition metal series might be expected to have a smooth dependence of the unresolved transition array (UTA) asymmetries and components upon the function of *Z*; and this would therefore be revealed in the experimental data. However, the coupling of valence electronic behavior and states (which leads to the satellite transitions) with unpaired *d* orbitals may be quite nonsmooth or even discontinuous for the *neutral metallic solid* target materials of investigation, as the outer electrons couple in the conduction band with 4*s* (and 4*p*) orbitals. Deciphering which aspect of theory dominates in the observed data is a key question of this paper.

A suitable highly resolved x-ray spectrum for vanadium is not available at present. Therefore, this work, using a high-precision medium-resolution crystal spectrometer, undertakes measurements of the spectrum for vanadium using a consistent basis with the other spectra. A complete and coherent picture, if any, of how emission line shapes evolve across atomic numbers $21 \leqslant Z \leqslant 25$, for the $K\alpha$ calibration lines, can then be made. While this paper critically reviews the past results, it also aims to provide a set of calibration standards for future experiments.

II. SPECTRAL SOURCE PROFILES AND PARAMETER MODELING

A full tabulation of characteristic lines and wavelengths was produced by Bearden *et al.* in the 1960s [17,18], in Å* units in the absence of the accurate transfer to the visible length scale. These also did not contain profiles, a separation of fitted components, or a defined spectrometer resolution relating the output peak channel locations to an underlying profile reference. Five *K* series spectral doublets were directly measured [19] but the remainder of the tabulation was formed from a critically reviewed and rescaled subset of earlier measurements. Of the five directly measured, only Cr $K\alpha_2$ is directly revelant to our current study, and this did not include, for example, Cr $K\alpha_1$. Hence the detailed profile information required is not present in these references for our use.

For the higher *Z* 3*d* transition metals, [15] provides detailed profiles for Cr (and Fe) and a detailed component analysis in terms of a sum of Lorentzians for Cr and Mn. That work separates five $K\alpha_1$ subcomponents and two $K\alpha_2$ subcomponents, each with energies, widths, amplitudes, and fitting uncertainties, and derives corresponding integrated peak intensities. Rather than providing a χ_r^2 result, these have provided a weighted *R* factor. The residual plots however indicate that these fits were fairly good and probably had a χ_r^2 close to unity. There is remaining structure in the residuals, implying that the convergence may not be complete, especially for the α_{12} and α_{13} components. Nonetheless the fits clearly represent the main features of the profile to high accuracy, and we use the fitted decomposition to define the original spectrum.

The plotted and fitted profiles for Cr and Mn are not the raw, experimental data collected; they have been deconvolved by an instrumental function representing the absorption path, collimator (divergence), and crystal diffraction

broadening. Hence they are approximations to an idealized purely atomic profile. Any real spectrum will be a broader convolution of this profile with an instrument function which may be symmetric, asymmetric, or complex. The generic case will not be a convolution but will be a more complicated function. The rays forming one part of the profile may not be broadened or modulated by the same instrument function as another part of the profile. In the case of the authors mentioned, the deconvolution was dominated by the beam divergence (as opposed to the asymmetric reflectivity), and the deconvolution was a 10% or less pseudo-Gaussian function. Hence the profiles were originally Voigt profiles, but the Gaussian component was deconvolved rather than being fitted. This removed part of the correlation between width parameters and assisted in the convergence to a fit with quite low parameter errors.

Given the deconvolution of these fits and plots, we might expect the results to show a χ_r^2 result significantly lower than unity, and to clearly define separate peaks for individual components. That this is not the case is probably healthy, in that (i) the unresolved transition multiplet and satellites are not well resolved, and hence by implication the intrinsic spectrum is only arbitrarily divided into seven components; and (ii) the location and widths of the weakest components are not well determined, but the spectrum is smooth, allowing us to usefully use and investigate the fitted deconvolved profiles.

For the scandium and titanium ($K\alpha$) profiles, detailed profiles are best provided by the team of Anagnostopoulos *et al.* [11,14]. These profiles are linked to the calibration route discussed earlier; but there has been no direct calibration of these profiles using an appropriate silicon standard. Therefore the absolute energy in scale and offset may be subject to a correction (of order the standard deviation, we believe, following [8]) when this step is completed. The profiles are given in raw data with counting statistic uncertainties. Hence we can expect some (pseudo-Gaussian or aperture function) instrument broadening to be present and potentially some asymmetry of peaks due to the intrinsic diffraction profile. Interestingly, the result of [14] is the only spectrum which is claimed to be limited by the intrinsic precision of the spectrum rather than by the absolute calibration of the energy axis.

Once again these are high-resolution spectra and imply that the instrument broadening is small compared to the profile width. The instrumental broadening can be well represented by a symmetric (Gaussian or aperture) broadening. Reduced χ_r^2 values are of order 1 for Sc and a similar unreported value for Ti $K\alpha$. In these two cases three $K\alpha_{1j}$ subcomponents and three $K\alpha_{2k}$ subcomponents are fitted by Voigt functions to include the instrument function, each with independent energies, Lorentzian widths, amplitudes and fitting uncertainties, with a common Gaussian (instrumental) width and with rough derived integrated peak intensities. The components are not tabulated for the Ti spectrum. However, the spectra include raw error bars for each point and the original spectrum is able to be reconstituted cleanly from the profile spectrum. We have therefore used the raw spectra with error bars. The fits of the Sc spectrum are labeled as three $K\alpha_1$ subcomponents and three $K\alpha_2$ subcomponents. The component labeled $K\alpha_{22}$ is conventionally labeled $K\alpha_{13}$ with the high energy component to $K\alpha_1$ being labeled $K\alpha_{14}$ or $K\alpha_{15}$. We use the conventional labels to provide a consistent comparison.

The capacity for even excellent spectra to determine more than six subcomponents for the $K\alpha$ spectrum is extremely dubious. We show below that it is unnecessary, that it appears to have yielded no significant reduction of χ_r^2, and that it is contraindicated by the data. We therefore use six subcomponents in our analysis.

There are many other observations of the spectrum of the Sc $K\alpha$ and Ti $K\alpha$, but we require high-resolution observations of the elemental profile (rather than the oxide, for example). The main published source of other high-resolution profiles is by the group of Kawai [20,21]. The earlier work [20] discusses widths, deconvolves the spectra, provides no component values and has no published good quality profile, so is not used in this work. However, the latter work provides useful quality spectra and the authors have also kindly provided some of their raw data. The processing prior to plotting included some smoothing and a background subtraction, but this does not affect widths and other parameters, so we make use of this raw spectrum. Point-wise uncertainties are dominated by counting statistics and are moderately well defined. The energy scale and offset are not rigorously determined by direct links to the lattice spacing transfer method, so the results are accurate to within an energy offset and scale correction. Hence we have two independent observations of the $K\alpha$ spectrum for Ti, and the consistency of results can be thereby investigated.

A key concern of this paper is to investigate these elemental spectra on a *uniform basis*, and in a form suitable for other medium (or low) resolution investigations, where the instrument function could be significant. The Lorentzian profile is the intrinsic line shape of a single transition line in both classical and quantum theory. Even in these high-resolution investigations, the raw data required a convolution of the (approximately Lorentzian) hole spectrum with an (approximately symmetric) instrumental function, which may be assumed to be Gaussian (representing Doppler, thermal, noise, and other broadening to yield a Voigt profile) or aperturelike (to yield a Lorentzian slit profile, hereafter referred to as an LS profile). A Voigt or LS profile will adequately represent most empirical broadenings and symmetric instrumental functions. In this paper we investigate the convergence and accuracy of the use of either function, applied to the good data described, as many researchers might use either convolved function for their analytical purposes. We do not investigate Voigt-slit or asymmetric profiles because (1) for good spectral conditions, this is unnecessary, and (2) the slit broadening and Gaussian broadening offer derivative signatures which are largely degenerate, leading to unphysical and meaningless conclusions.

There is no detailed profile spectrum of vanadium $K\alpha$ in the literature, for calibration transfer or to investigate the consistency of the series of open d shell spectra in this range. Accordingly, we have measured the vanadium spectra to medium resolution. Our measurement is a relative one and the calibration of the peaks is given by the original processed reports; however, this profile analysis allows the trends of

spectra and relative shifts and satellites to be investigated robustly.

III. EXPERIMENTAL: VANADIUM

Measurements were performed at an electron beam ion trap (EBIT) using a x ray Johann curved-crystal focusing spectrometer with position-sensitive detection at the National Institute of Standards and Technology (NIST). Curved crystal spectrometry can achieve a precision of less than 5 ppm because the focusing ability of the crystal increases the efficiency of the spectrometer and improves resolution for broad or diffuse sources. The stability of the position of the focal point of the x rays on the Rowland circle with respect to the source motion is high compared to other techniques. This stability is particularly important since the EBIT location may drift over time due to mechanical shifts from the thermal expansion and contraction of the EBIT apparatus components or the focusing of the electron gun and electronics. Such drifts may be of magnitude of ± 10 μm perpendicular to the axis to electron beam [22], which would affect the location of peaks in flat crystal focussing; the spectroscopic method adopted here is insensitive to such shifts, even if of a much larger magnitude.

The distance of the detector [in this case a specialized backgammon detector [23] with effective resolution element (pixel size) of circa 49 μm], to the crystal employed is chosen so that the Rowland circle, [radius 1.089 m, defined by crystal curvature of (2.178 ± 0.005)m], is large enough to encompass both the EBIT and calibration sources. Such an arrangement enables us to obtain spatially well separated spectral lines and increases the collecting power, approaching the geometric relation (flux $\propto 1/D^2$, where D is source-to-crystal pole distance). The V $K\alpha$ lines are in focus at the position of the detector.

IV. Sc, Ti, Cr, AND Mn $K\alpha$ COMPONENT REFITTING

We need to refit and reanalyze Sc, Ti, Cr, and Mn $K\alpha$ spectra in order to consider trends in satellite production and profile shapes. Refittings using Voigt profiles and six components are given in Table I. Vanadium is included here as determined below for completeness and comparison.

Six peaks are fitted to the spectrum corresponding to the $K\alpha_1$ diagram line (labeled $K\alpha_{11}$), the $K\alpha_2$ diagram line (labeled $K\alpha_{21}$), lower energy $K\alpha_1$ satellites ($K\alpha_{12}$, $K\alpha_{13}$), a higher energy $K\alpha_1$ satellite ($K\alpha_{14}$), and a lower energy $K\alpha_2$ satellite ($K\alpha_{22}$).

The spectrum may be given as a sum of Voigt profiles with a common Gaussian width w_G representing the instrumental broadening, where $w_{L_{jk}}$ is the Lorentzian width of the jk component, c_{jk} is the centroid location of that component in the same arbitrary units, x_i is the channel of interest of the spectrum, and x is the convolution variable

$$F(x_i) = \sum_{\alpha_{jk}} \int_{2.5w_G}^{2.5w_G} \frac{w_{L_{jk}}^2/4}{(x_i - c_{jk} - x)^2 + w_{L_{jk}}^2/4} dx. \qquad (1)$$

Our earlier scepticism in the ability of high-resolution experiments to separate seven components cleanly (relating to specific real satellite structure as opposed to merely an empirical fit without deeper significance) is demonstrated in the tables. Even with only six components, the matrix is highly correlated and the separation of peaks is nontrivial. The physical understanding of the diagram lines ($K\alpha_{11}$, $K\alpha_{21}$) and the high energy and low energy peaks ($K\alpha_{15}$, $K\alpha_{22}$) is relatively straightforward; but the clean separation of the last two components ($K\alpha_{12}$, $k\alpha_{13}$) from one another is less clear, given that theory predicts complex multiplets of variable amplitudes. In all these spectra six components are needed to obtain a good χ_r^2.

The very weak component $K\alpha_{22}$ is (relatively) poorly determined (Table I). The fit requires such a component, but it has small and highly variable amplitudes, and often broad and imprecise widths. The small peaks "in the middle," $K\alpha_{13}$ and $K\alpha_{12}$, are also relatively imprecise, as should be expected. These imprecisions do not affect the final result or, for example, the accuracy of the identification of the (Bearden or Deslattes) peak locations ($K\alpha_1^0$, $K\alpha_2^0$).

We can only compare our results to those of the original literature for Sc, Cr, and Mn; all other results are completely new in this paper. For Ti [14], profile analysis was not done; for Ti [21] neither profile analysis nor absolute calibration was performed; and of course for vanadium there was no data. Hence we present the profile fits and residuals in Figs. 1–5. These figures permit others to reanalyze the fits further.

In Tables I and II, units are in eV or counts, although for Cr and Mn [15] the published spectrum was already deconvolved, so the counts are not quite representative of the true counting statistics of the original raw data. Energies and widths listed have been defined by Deslattes *et al.* [24] and the sources listed in the tables. Uncertainties in the tables and figures are one standard deviation fitting precisions for the particular component and parameter listed. These parameters are highly correlated, so that lower uncertainties would be reported after deconvolution or upon the removal of a free parameter. Although some parameter uncertainties might seem relatively large, the consequent uncertainty of the profile fit (and hence of the χ_r^2) is much smaller, and hence the determination of the peak postion is highly accurate in all cases.

The results for Sc [11] are completely consistent with our results within one standard deviation except for the position and hence width and amplitude of $K\alpha_{13}$. This discrepancy is about 2.5 standard deviations, but relates to the most poorly defined peak. The original reference did not fit the Gaussian width; instead it was constrained or reported without error. Our result appears to have a lower χ_r^2 and is therefore a "better fit;" but the error bars of the original reference fit are somewhat lower (sometimes by a factor of two) because of the suppression of the correlation between the Gaussian width parameter and all other coefficients. This is fully consistent, and we restate our aim: to provide a uniform and consistent set of data across atomic number in order to investigate trends and determine a reliable and robust result for vanadium, and for calibration of the whole series, particularly as a transfer standard to lower resolution spectral determinations.

TABLE I. Centroids C_i, widths W_i, amplitudes A_i, and (derived parameter) integrated intensities I_i of individual components obtained from fitting six Voigts to $K\alpha_{1,2}$ emission profiles of elemental targets of Sc through Mn.

Element	Peak i	Centroid C_i (eV)	Width W_i (eV)	Amplitude A_i (counts)	Integrated intensity I_i[a] (counts)	Source (other parameters)
Sc	α_{11}	4090.745(7)	1.17(5)	8175(166)	106068(5362)	Refit of [11]
	α_{12}	4089.452(192)	2.65(44)	878(128)	22424(4948)	Anagnostopoulos *et al.* (1999)
	α_{13}	4087.782(104)	1.41(95)	232(101)	3474(2781)	Gaussian width=0.52(6) eV
	α_{15}	4093.547(61)	2.09(20)	387(21)	7993(867)	
	α_{21}	4085.941(9)	1.53(7)	4290(60)	68142(3238)	
	α_{22}	4083.976(541)	3.49(70)	119(45)	3585(1546)	χ_r^2=0.44
Ti	α_{11}	4510.926(14)	1.32(11)	579(12)	28582(2527)	Refit of [14]
	α_{12}	4509.467(141)	1.54(47)	73(28)	4064(1976)	Anagnostopoulos *et al.* (2003)
	α_{13}	4507.735(217)	2.77(93)	42(9)	3717(1498)	Gaussian width=0.68(14) eV
	α_{15}	4513.848(109)	1.75(28)	30(3)	1793(352)	
	α_{21}	4504.914(20)	1.73(16)	272(8)	16280(1614)	
	α_{22}	4502.611(566)	3.30(106)	15(5)	1345(637)	χ_r^2=1.01
Ti	α_{11}	4510.918(10)	1.37(5)	4549(199)	236462(13010)	Refit of [21]
	α_{12}	4509.954(174)	2.22(52)	626(192)	51234(19831)	Kawai *et al.* (1994)
	α_{13}	4507.763(282)	3.75(94)	236(57)	31098(10849)	Gaussian width=0.11(16) eV
	α_{15}	4514.002(40)	1.70(14)	143(7)	8839(849)	
	α_{21}	4504.910(7)	1.88(4)	2034(24)	143328(3673)	
	α_{22}	4503.088(599)	4.49(71)	54(19)	8097(3116)	χ_r^2=1.04
V	α_{11}	4952.237(12)	1.45(2)	25832(473)	363716(7705)	This work
	α_{12}	4950.656(184)	2.00(3)[b]	5410(53)[b]	88933(1451)	
	α_{13}	4948.266(261)	1.81(70)	1536(316)	24142(4972)	Gaussian width=1.99(12) eV[b]
	α_{15}	4955.269(141)	1.76(30)	956(92)	14216(1370)	
	α_{21}	4944.672(21)	2.94(4)	12971(101)	264892(3901)	
	α_{22}	4943.014(303)	3.09(26)	603(48)[b]	12721(1466)	χ_r^2=0.91
Cr	α_{11}	5414.851(3)	1.415(3)	10370(22)	221241(618)	Refit of [15]
	α_{12}	5413.924(12)	2.332(15)	2936(11)	100678(731)	Holzer *et al.* (1997)
	α_{13}	5411.565(40)	6.234(37)	889(3)	73157(517)	Gaussian width=0.00924(2) eV
	α_{15}	5418.357(84)	1.05(10)	109(9)	1714(212)	
	α_{21}	5405.531(5)	2.292(3)	5011(13)	168311(497)	
	α_{22}	5402.696(80)	3.554(84)	194(4)	306(9)	χ_r^2=0.88[c]
Mn	α_{11}	5898.855(5)	1.627(4)	7942(24)	192934(720)	Refit of [15]
	α_{12}	5897.739(11)	2.195(8)	3008(12)	97304(532)	Holzer *et al.* (1997)
	α_{13}	5895.612(23)	4.34(2)	1152(4)	69664(362)	Gaussian width=0.00982(1) eV
	α_{15}	5899.400(85)	1.89(6)	384(8)	10738(404)	
	α_{21}	5887.711(5)	2.511(4)	4224(6)	151862(324)	
	α_{22}	5885.967(41)	4.19(3)	626(3)	33546(252)	χ_r^2=0.42[c]

[a]This is a derived parameter.
[b]These parameter uncertainties were constrained as with the Gaussian width in other work to avoid singular values.
[c]Cr and Mn spectra were reconstructed from the fitted peak profiles, therefore neglecting noise contributions, so $\chi_r^2 < 1$.

The results for Cr and Mn are similar, and also generally within one standard deviation for the parameters involved. Those authors deconvolved the Gaussian, so the original error bars are smaller than those in the tables, where a Gaussian width has been separately parametrized. Hence the Gaussian component is virtually zero as stated by the original authors, after deconvolution, of course.

Two anomalies should be discussed. In the original reference [15], the width of the Mn $K\alpha_{15}$ component was less than that of the diagram line. In our refit this is not the case.

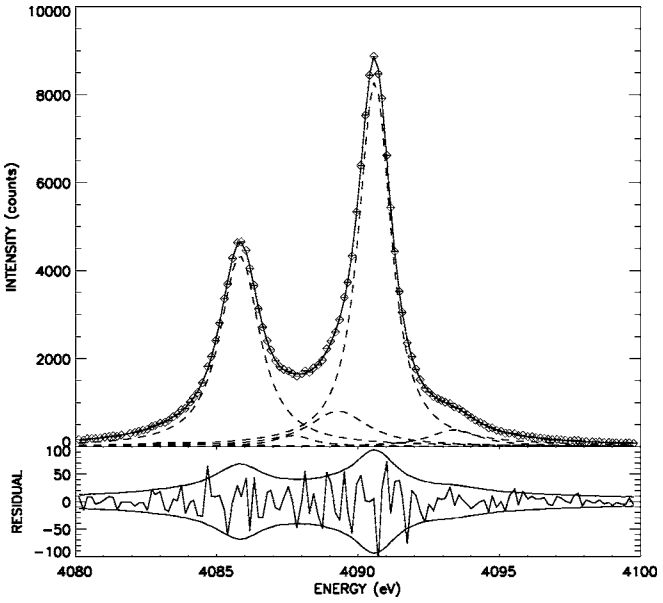

FIG. 1. Profiles and residuals for Sc $K\alpha$, $Z=21$, Ref. [11] fitted with Voigt profiles (remodeled).

Any physical satellite is expected to have a width broader than the diagram line (no metastable transitions have a significant amplitude). This is a sign that the original fit does not determine this component in a clean uncorrelated manner. In part this is a justification for using one less component. However, for Cr $K\alpha_{15}$, the original source yielded a possibly physical width for this component; yet our reanalysis yields a width which is too narrow. Hence, the signature for this $K\alpha_{15}$ peak is weakly determined. The peak itself is clearly in the data; but because it is so weak the parametrization is significantly affected by the $K\alpha_{11}$ peak parameters and especially the $K\alpha_{11}$ width. We conclude that all parameters are determined consistently and uniformly, but that minor effects as just discussed will be revealed in the trends.

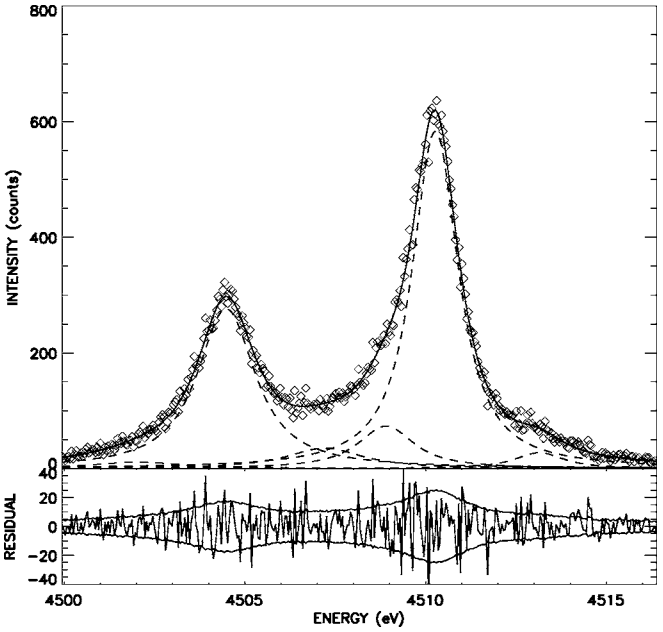

FIG. 2. Profiles and residuals for Ti $K\alpha$, $Z=22$, Ref. [14] fitted with Voigt profiles.

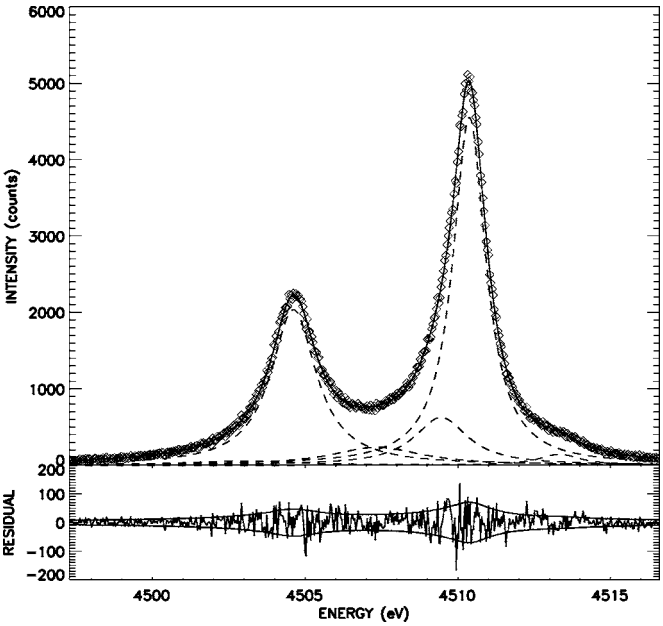

FIG. 3. Profiles and residuals for Ti $K\alpha$, $Z=22$, Ref. [21] fitted with Voigt profiles.

We defer discussion of vanadium to the section below. According to Table I, Kawai *et al.* [21] and Anagnostopoulos *et al.* [14], Ti $K\alpha$ measurements yield apparent differences in components fitted. There are as much as 0.9 eV and 1.4 eV differences in the centroid and width of the $K\alpha_{22}$ component. This suggests different experimental conditions have significantly impacted upon the significance of the weaker satellites.

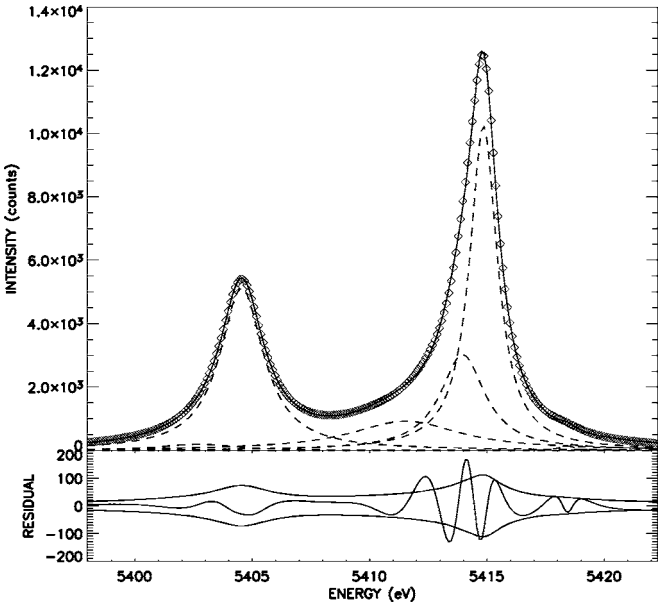

FIG. 4. Profiles and residuals for Cr $K\alpha$, $Z=24$, Ref. [15] fitted with Voigt profiles (remodeled).

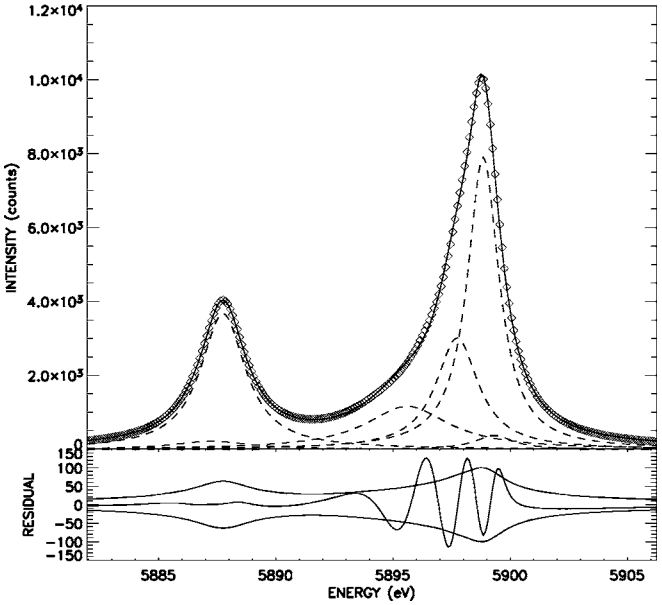

FIG. 5. Profiles and residuals for Mn $K\alpha$, $Z=25$, Ref. [15] fitted with Voigt profiles (remodeled).

V. COMPONENT REFITTING WITH LORENTZIAN-SLIT PROFILES

In order to compare the result of fitting different functional forms (Voigts and Lorentzian-slit profiles), the above measurements are fitted accordingly with six Lorentzian-slit profiles, whose results are given in Table II.

The LS fits have similar values for χ_r^2, as should be expected for high-resolution profiles dominated by natural and diffraction broadened linewidths with minimal Gaussian or aperture broadening. On the basis of Tables I and II, both profiles are generally similar and hence robust, and users could use either to reproduce high-resolution double-flat crystal profiles. The LS profile fits and residuals are presented in Fig. 6–10.

All spectra were measured under similar conditions (namely a double flat spectrometer) to those of Ref. [17] and hence should involve consistent definitions of the $K\alpha$ peaks (with the obvious exception of vanadium). Uncertainties in this definition of the energy axis are given by these sources and summarized in Table III.

VI. DETERMINATION OF ESTIMATED INITIAL PARAMETERS AND CONSTRAINTS FOR VANADIUM

In an instrumentally broadened system, component parameters are highly correlated with one another, but using intelligent estimates should converge to a global minimum reflecting the physical solution or disproving the assumptions made. Finding the consistent solution, as in this analysis, is a strong indication that the true minimum has been approached successfully.

The general strategy for determining initial parameter values for fitting a deconvoluted profile is to predict the characteristic quantity ratios of the six fitting components. This is based on the hypothesis (at this stage) that trends exist. The method of interpolation for vanadium is by fitting a linear or polynomial (quadratic) trend to the adjacent data points. The result is clear and obvious.

Investigation of how the characteristic satellite structures evolve with Z is made by computing derived ratios relative to the scales of the offsets and fine structure. Width ratios $W_{\alpha_j}/W_{\alpha_{11}}$, integrated intensity ratios $I_{\alpha_{jk}}/I_{\alpha_{11}}$, $jk=12$, 13, 15, 21, and 22, and centroid coefficient ratios defined by

$$R_{\alpha_{jk}} = \frac{C_{\alpha_{jk}} - C_{\alpha_{11}}}{C_{\alpha_{21}} - C_{\alpha_{11}}}, \quad jk = 12,13,15,22, \tag{2}$$

are used, calculated and plotted with a linear or polynomial fitting function. Here, $C_{\alpha_{jk}}$ is the energy of the peak of the jk component. The Gaussian (G), Lorentzian (L), and slit (S) widths for $W_{\alpha_{11}}$ can also be normalized to the scale of the structure to give indications of normalized separations of the components

$$\frac{G_{\alpha_{11}}}{C_{\alpha_{21}} - C_{\alpha_{11}}}. \tag{3}$$

From these values, a plausible range of these parameter ratios across the range of Z may be investigated. The ratios detail progressive structural development with Z and offer useful estimates for the search for the best fit in the correlated parameter space.

Estimates of the 19 parameters based on linear or quadratic interpolation vary significantly, but usually with a clear preference on the basis of the best fit. The fitted parameter value was relatively insensitive to this initial estimate, so long as the estimates lay within a broad range. Estimates based on Voigt or LS profile fitting are largely consistent, so do not affect any *a priori* estimates.

VII. VANADIUM FITTING

In the second step of the vanadium analysis, fast Fourier transform deconvolution by a Gaussian response function is used to determine the "true" (approximately instrument free) emission line profile. In doing so, noise in the form of Fourier spikes can be introduced into the deconvolved profile. This is a typical tradeoff when doing fast Fourier transforms numerically with finite step size and frequency range. By zeroing such spurious frequencies, a clean profile is acquired, with a very minor loss of information content, but with the same clarification of peak and subcomponent structure as was obtained by [15].

The profile can be fitted using the Levenberg-Marquardt curve fitting algorithm for all parameters, using as initial estimates the predictors of the previous section; but particularly noting the clean determinations of integrated intensity ratios $I_{\alpha_{12}}/I_{\alpha_{11}}$, $I_{\alpha_{21}}/I_{\alpha_{11}}$ and width ratios $W_{\alpha_{12}}/W_{\alpha_{11}}$, and by comparison to the estimated ratios. Subsequent fits yield a χ_r^2 for the deconvolved spectrum of 0.66 where χ_r^2 is the least squares fitting criterion, defined in Eq. (4). The weighting follows the counting statistics, $W_i=1/Y_i$, and standard deviation for counting statistics is $\sigma=1/\sqrt{N}$

TABLE II. Centroids C_i, widths W_i, amplitudes A_i, and (derived parameter) integrated intensities I_i of individual components obtained from fitting six Lorentzian slit (LS) profiles to $K\alpha_{1,2}$ emission profiles of elemental targets of Sc through Mn.

Element	Peak i	Centroid C_i (eV)	Width W_i (eV)	Amplitude A_i (counts)	Integrated intensity I_i[a] (counts)	Source (other parameters)
Sc	α_{11}	4090.595(6)	1.13(4)	8203(155)	101638(3906)	Refit of [11]
	α_{12}	4089.308(169)	2.46(48)	818(124)	19403(4821)	Anagnostopoulos *et al.* (1999)
	α_{13}	4087.666(161)	1.58(93)	257(104)	4159(2974)	Slit width=0.66(6) eV
	α_{15}	4093.428(52)	2.04(18)	381(19)	7607(767)	
	α_{21}	4085.773(8)	1.94(5)	4299(54)	66523(1960)	
	α_{22}	4083.697(493)	3.42(72)	105(32)	3065(1143)	χ_r^2=0.48
Ti	α_{11}	4510.937(22)	1.39(8)	582(15)	29173(1816)	Refit of [14]
	α_{12}	4509.485(133)	1.41(116)	67(32)	3399(3242)	Anagnostopoulos *et al.* (2003)
	α_{13}	4507.854(579)	2.89(167)	43(22)	3904(3005)	Slit width=0.82(14) eV
	α_{15}	4513.907(92)	1.66(28)	29(3)	1598(309)	
	α_{21}	4504.908(20)	1.81(15)	273(9)	16534(1478)	
	α_{22}	4502.510(544)	3.17(109)	13(4)	1130(524)	χ_r^2=1.00
Ti	α_{11}	4510.901(10)	1.36(5)	4550(199)	236480(12978)	Refit of [21]
	α_{12}	4509.940(173)	2.21(52)	626(192)	51208(19804)	Kawai *et al.* (1994)
	α_{13}	4507.757(281)	3.74(93)	236(57)	31099(10828)	Slit width=0.15(22) eV
	α_{15}	4513.975(39)	1.70(14)	143(7)	8831(847)	
	α_{21}	4504.911(7)	1.88(4)	2034(24)	143370(3649)	
	α_{22}	4503.092(597)	4.48(70)	54(19)	8073(3105)	χ_r^2=1.04
V	α_{11}	4952.224(18)	1.73(5)	25807(381)	371815(11443)	This work
	α_{12}	4950.398(147)	2.10(27)	5460(1003)[b]	87050(19642)	
	α_{13}	4947.434(184)	2.22(192)	1641(554)	27144(25144)	Slit width=2.24(3) eV
	α_{15}	4954.420(173)	1.82(34)	1336(289)	19287(5494)	
	α_{21}	4944.652(48)	2.96(8)	12893(466)	252420(11491)	
	α_{22}	4942.372(152)	2.30(30)	642(581)[b]	10634(9711)	χ_r^2=3.02
Cr	α_{11}	5415.536(3)	1.501(3)	9940(24)	21270(2)	Refit of [15]
	α_{12}	5414.658(12)	2.378(12)	3275(9)	10657(1)	Holzer *et al.* (1997)
	α_{13}	5412.284(38)	5.44(3)	1004(4)	7049.422(3)	Slit width=0.0500(1) eV
	α_{15}	5419.275(63)	1.34(4)	151(11)	276.79819(4)	
	α_{21}	5405.512(5)	2.643(2)	5000(15)	17660.94(96)	
	α_{22}	5402.060(96)	3.33(13)	148(2)	494.87(27)	χ_r^2=0.70[c]
Mn	α_{11}	5898.858(5)	1.628(2)	7911(32)	192333(820)	Refit of [15]
	α_{12}	5897.751(12)	2.193(7)	3015(15)	97436(569)	Holzer *et al.* (1997)
	α_{13}	5895.63(3)	4.36(2)	1163(6)	70650(481)	Slit width=0.001000(1) eV
	α_{15}	5899.39(9)	1.86(4)	378(7)	10388(274)	
	α_{21}	5887.740(5)	2.407(4)	3672(12)	145825(344)	
	α_{22}	5885.93(4)	3.81(2)	216(3)	34395(242)	χ_r^2=0.41[c]

[a]This is a derived parameter.
[b]These parameter uncertainties were constrained as with the Gaussian width in other work to avoid singular values.
[c]Cr and Mn spectra were reconstructed from the fitted peak profiles, therefore neglecting noise contributions, so $\chi_r^2 < 1$.

$$\chi_r^2 = \Sigma_{i=1}^{N_Y} \frac{W_i (Y_i - F_i)^2}{N_{\text{free}}}. \quad (4)$$

The fitted parameters can then be used as the initial parameters for fitting six Voigts to the raw vanadium spectrum (i.e., including the instrumental broadening), illustrated in Fig. 11. The prediction based upon structural trends across atomic number yielded the same answer in a more efficient manner, so that with good data this earlier step was an unnecessary but useful cross check on the robustness and sta-

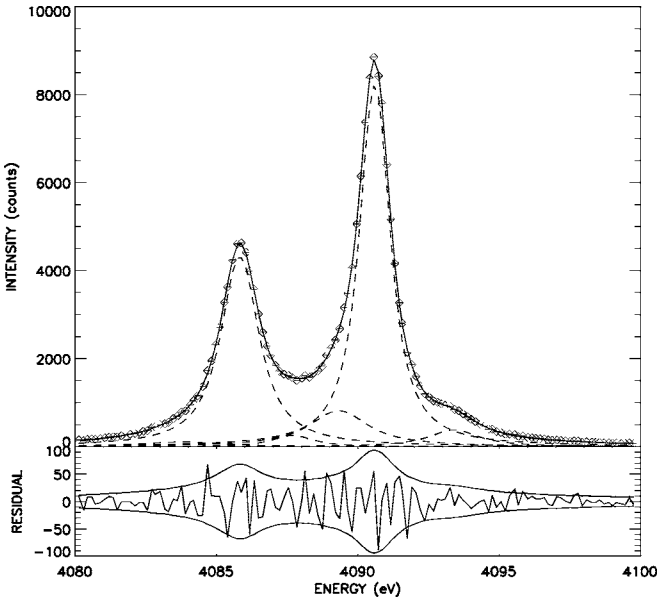

FIG. 6. Profiles and residuals for Sc $K\alpha$, $Z=21$, Ref. [11] fitted with LS profiles (remodeled).

bility of the results. An examination of the valley of χ_r^2 by fitting with different sets of fixed centroids proves that the centroid of $K\alpha_{12}$ is a key component in shaping the quality of the fit.

We have implemented a very efficient Voigt fitting routine for these correlated spectra which includes a rapid lookup table for the range of possible normalized Voigt profile shapes. This is on average much faster than a typical integrating fitting routine, and converges to a lower final χ_r^2 in many cases.

Lorentzian-slit functions are often used to represent broadened profiles. The LS function is practical and efficient

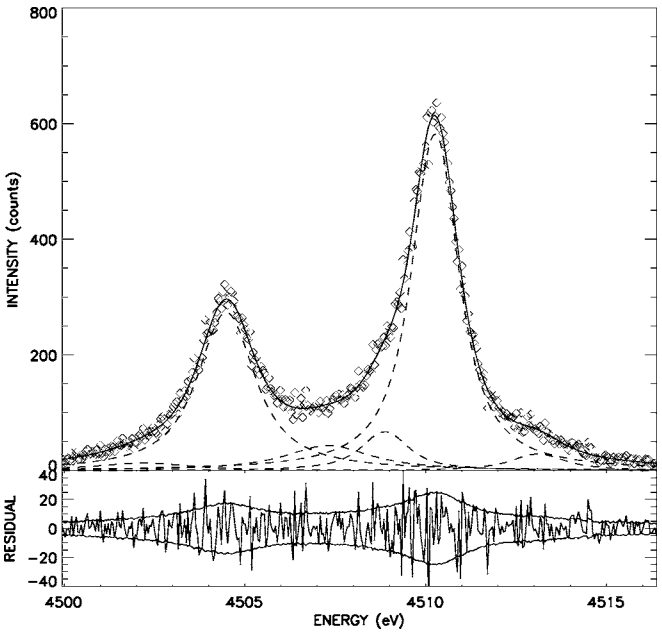

FIG. 7. Profiles and residuals for Ti $K\alpha$, $Z=22$, Ref. [14] fitted with LS profiles.

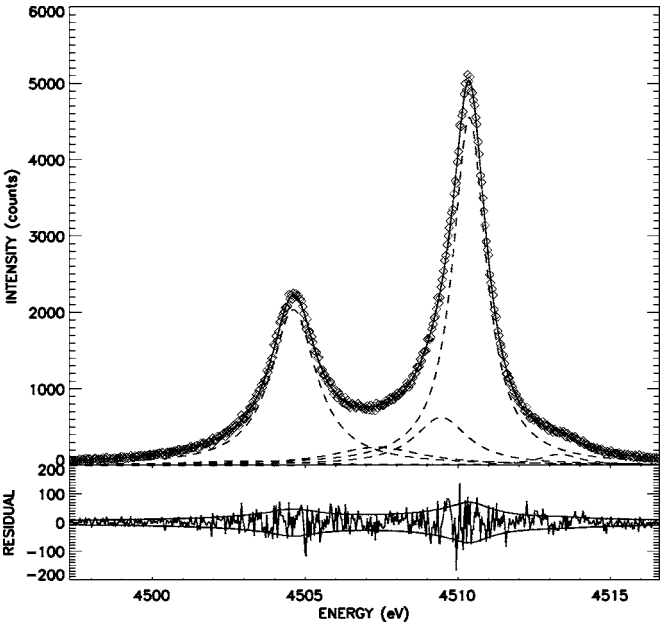

FIG. 8. Profiles and residuals for Ti $K\alpha$, $Z=22$, Ref. [21] fitted with LS profiles.

and has a well-known functional form with the same set of components as given in Eq. (4). The model achieves a fit with a χ_r^2 of 3.02, significantly poorer than the result of $\chi_r^2=0.91$ for Voigt profile analysis. The χ_r^2 fit of the profile tails forces discrepancies at the peaks. This implies that the extended tails of the spectrum are Voigt like and that the additional broadening is dominated by a Gaussian character rather than a slit character. This conclusion is confirmed by a comparison of the values and uncertainties of the LS fit compared to that of the Voigt fitting.

The signature of the residual structure of the LS profile fit agrees with that of Voigt fitted result but differs particularly

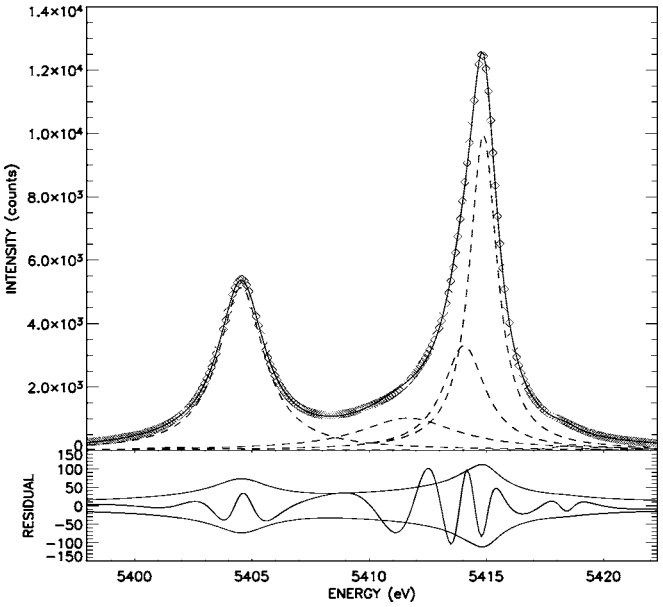

FIG. 9. Profiles and residuals for Cr $K\alpha$, $Z=24$, Ref. [15] fitted with LS profiles (remodeled).

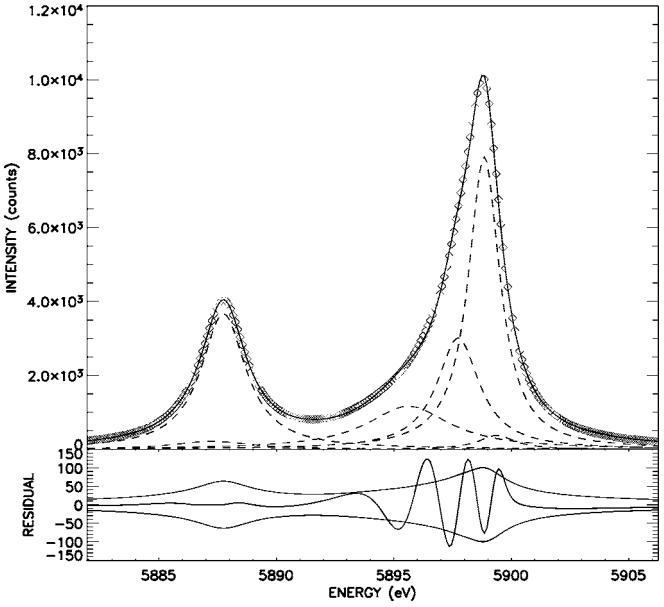

FIG. 10. Profiles and residuals for Mn $K\alpha$, $Z=25$, Ref. [15] fitted with LS profiles (remodeled).

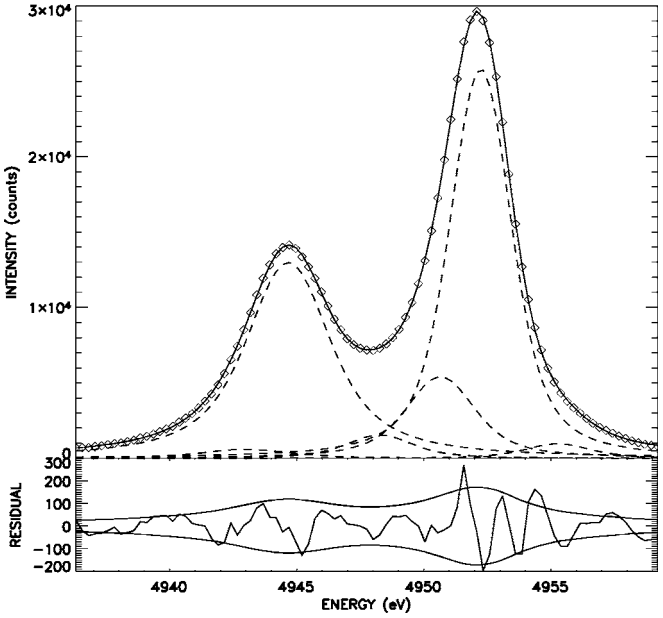

FIG. 11. Profiles and residuals for V $K\alpha$, $Z=23$, fitted with Voigt profiles (this work) $\chi_r^2=0.91$. The x axis is corrected (scaled to the absolute determination) including all effects discussed in the text.

in the peak region due to the profile inadequacies (Fig. 12). The final fit parameters of both approaches are tabulated in Tables I and II, respectively.

VIII. DETERMINATION OF $K\alpha_{jk}$ AND $K\alpha_i^0$ ENERGIES

The uncertainty of the component parameter output represents the ability of the data and fitting routines to separate the component oscillations from the unresolved profile (Tables I and II). This includes the ability to determine an accurate energy to a subcomponent which is generally not so well determined, and not so important either, given the discussion above.

The $K\alpha_1^0$ and $K\alpha_2^0$ positions directly determine the offset and scaling, and so have no meaning in the relatively scaled sense. The uncertainty in the final energies of these gives the full profile registration and the limiting uncertainty in derived energies. Therefore $K\alpha_1^0$ and $K\alpha_2^0$ positions, based on the peak uncertainties and the uncertainties from the direct link to the meter, are robust indicators of the transfer process and the final uncertainties of the calibration procedure. Final error estimates can involve double counting of the contributing errors (if they arise from the same source) but our estimates are therefore robust.

For Sc, Ti, Cr, and Mn, the energies of $K\alpha_1^0$ and $K\alpha_2^0$ are given by the the positions of maximum amplitudes of the analytic representation of the profile, as summarized in Table III. The most comprehensive summary of experimental measurements of $K\alpha_1^0$ and $K\alpha_2^0$ energies in eV for these elements is given in Deslattes *et al.* [24]. The channel centroids of all the components are calibrated by Eq. (5)

$$E_{\alpha_j} = (C_{\alpha_{jk}} - C_{\alpha_1^0}) f_{calib} + E_{\alpha_1^0}, \tag{5}$$

where the scale factor $f_{calib}=(E_{\alpha_1^0}-E_{\alpha_2^0})/(C_{\alpha_1^0}-C_{\alpha_2^0})$ and $C_{\alpha_{jk}}$ are in units of channel numbers (or any other linear measure). Deslattes *et al.* energies are directly applicable to these four elements because the profile spectrum has identical or almost equal resolution to the energy peak determination for each element. In the original documents the statistical error of the calibration is dominated by the accuracy of the overall energy scale for Cr, Mn, and Sc, while in the case of Ti the statistical error is dominant. This is clearly stated in the ref-

TABLE III. Experimental energy determinations in eV for the peak values $K\alpha_1^0$, $K\alpha_2^0$ used in determining the absolute scale of energy, from Ref. [24] including the source data for Ref. [14].

Element	$K\alpha_1^0$	$\sigma(K\alpha_1^0)$	$K\alpha_2^0$	$\sigma(K\alpha_2^0)$	Reference
Sc	4090.735	0.019	4085.9526	0.0085	[24]
Ti	4510.8991	0.0094	4504.9201	0.0094	[24]
Ti	4510.903	0.019(0.011)	4504.942	0.040(0.011)	[14]
V	4952.216	0.059	4944.671	0.059	[24]
Cr	5414.8045	0.0071	5405.5384	0.0071	[24]
Mn	5898.801	0.0084	5887.6859	0.0084	[24]

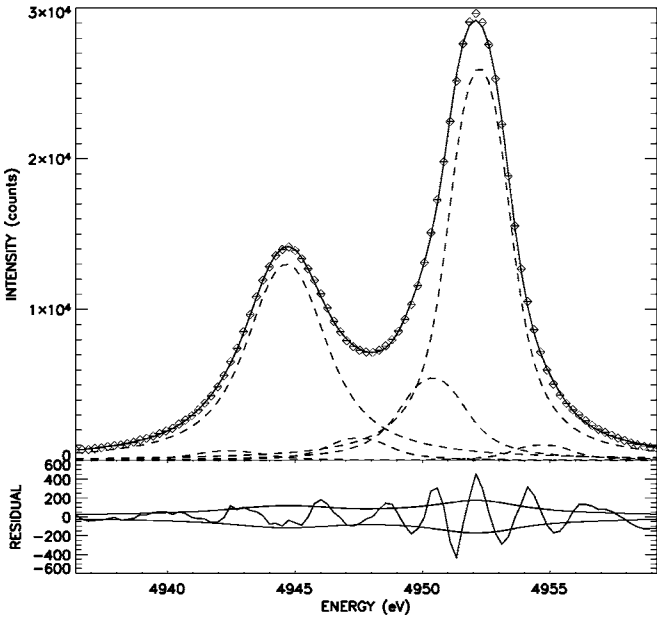

FIG. 12. Profiles and residuals for V $K\alpha$, $Z=23$, fitted with LS profiles (this work). $\chi_r^2=3.02$. The x axis is corrected (scaled to the absolute determination) including all effects discussed in the text.

erences. The final uncertainty for [24] is lower than for the source reference [14] because the compiled value is a weighted mean of this source and the earlier Bearden result. We list both in Table III for completeness.

For error analysis, the uncertainties in Deslattes *et al.* energies may be transfered to the assignment of energy to a particular channel E_x to obtain self-consistent uncertainties in component energies and widths, by Eq. (7)

$$E_x = (1-a_x)\times E_{\alpha_1^0} + a_x \times E_{\alpha_2^0}, a_x = \frac{C_x - C_{\alpha_1^0}}{C_{\alpha_2^0} - C_{\alpha_1^0}}, \qquad (6)$$

and assuming independent errors

$$\delta E_x = \sqrt{(1-a_x)^2 \times \delta E_{\alpha_1^0}^2 + a_x^2 \times \delta E_{\alpha_2^0}^2}. \qquad (7)$$

Similiar treatment can be made to the vanadium measurement in this work. However, the experimental resolution reported here for vanadium is lower than that for the (Bearden and Deslattes) references. This is directly due to the broader instrumental function and hence (to first order) from the significantly larger Gaussian width in the Voigt profile.

It is necessary to examine the consequent shift of $K\alpha_1$ and $K\alpha_2$ positions at Gaussian widths (i.e., broadening) varying from the explicit experimental profile values down to the resolution corresponding to the literature determination of the peak positions. Essentially, a Voigt profile with an explicitly reduced Gaussian width represents a spectrum deconvolved from the Gaussian response function. The experimental resolution is worse than Deslattes *et al.* by approximately a factor of two. However, the other profiles have a Lorentzian width for the diagram line ($K\alpha_1^0$, or equally $K\alpha_{11}$) which is stable and smooth. Interpolation here implies that the corresponding double flat crystal Lorentzian width for vanadium is expected to be 1.39 eV. An uncertainty may be taken from the smoothness of the trend, the individual width uncertainties for $K\alpha_{11}$ and from minor variation of widths from the two titanium results. This implies a Lorentzian width uncertainty of approximately 0.03 eV.

The expected Gaussian or slit widths (depending upon the profile assumed) are less well determined, particularly since some of the earlier literature has fixed or deconvolved this width. There is a range from perhaps 0.51 eV to 0.8 eV for the representation of the resolution and profile obtained from a double flat or high resolution crystal monochromation. However, there is a consistent estimate from this of 0.6 eV, particularly if we include a "one standard deviation" uncertainty of 0.1 eV. These are then the values modeled in Table IV.

The corresponding shifts of the peak of the raw spectrum, with respect to the deconvolved spectrum, are 0.013 eV for $K\alpha_1^0$ and 0.004 eV for $K\alpha_2^0$. The shift is definitely significant, but extremely stable. Large variations of the widths around these expected locations do not change the location of the peak position. The largest shift is for $K\alpha_1^0$ despite the better statistics, because of the influence of the nearby $K\alpha_{12}$ component.

TABLE IV. Shifts ΔC and one standard deviation uncertainty contributions $\sigma(\Delta C)$ to the determination in eV for the peak values $K\alpha_1^0$, $K\alpha_2^0$ for vanadium, in addition to 0.059 eV for the reference location uncertainty, including the resolution correction. Expected widths of Lorentzian L=(1.39±0.03) eV, and Gaussian (or slit) G or S=(0.6±0.1) eV are derived from the consistency and trend of the double flat crystal measurements for Sc, Ti, Cr, and Mn.

Centroid shifts for vanadium ΔC, $\sigma(\Delta C)$(eV)				
Resolution mismatch	ΔC $K\alpha_1^0$	$\sigma(\Delta C)$ $K\alpha_1^0$	ΔC $K\alpha_2^0$	$\sigma(\Delta C)$ $K\alpha_2^0$
V, Voigt fit	−0.085	0.006	−0.020	0.011
V, LS fit	−0.1025	0.011	−0.003	0.0235
Precision of $K\alpha_1^0$, $K\alpha_2^0$ for a single (backgammon) image		0.0034		0.0068
Indicative statistical precision for $K\alpha_1^0$, $K\alpha_2^0$: FWHM/$\sqrt{N}$		0.005		0.009

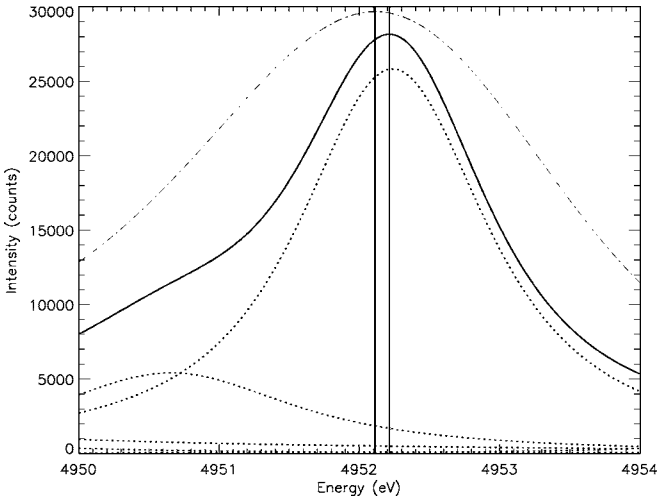

FIG. 13. Shifts of V $K\alpha_1^0$ (vertical solid line) of the deconvolved (Voigt) spectrum (solid curve and dotted subcomponent amplitudes) compared to the experimental profile and width (dot-dash curve and vertical line), as summarized in Table IV. The scale is expanded in order to demonstrate the shift between the two "results" for $K\alpha_1^0$ as a consequence of the additional broadening.

Figures 13 and 14 show the raw data, the deconvolved spectra (a much simpler process than the fast fourier transform (FFT) deconvolution), and the consequent shift of the peak location, expanded for clarity. Comparing with the direct uncertainty of $K\alpha_{1,2}^0$ reported in the literature for vanadium, the corresponding uncertainties in the shifts are smaller by a minimum factor of 4. The uncertainty for profiles fitted with LS profiles is about double that for the Voigt profile results, due to the poorer fits and larger fitting errors, but these two results are consistent. Hence, this correction is inconsequential to the final error budget and thus the error is a minor contribution to the final result.

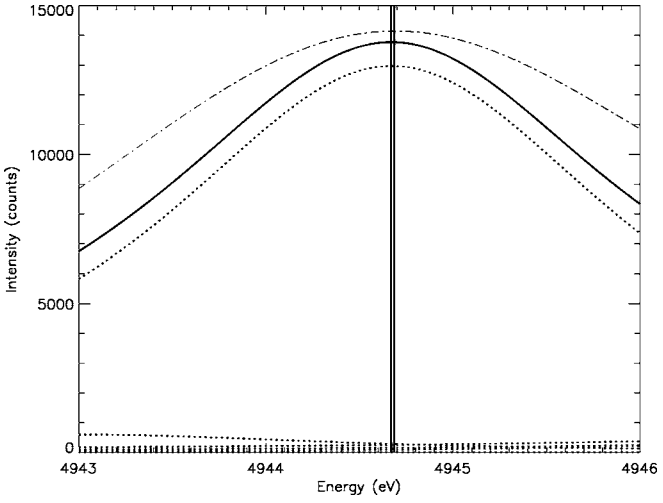

FIG. 14. Shifts of V $K\alpha_2^0$ (solid vertical line) of the deconvolved (Voigt) spectrum (solid curve and dotted components) compared to the experimental profile and width (dot-dashed curve and vertical line), as summarized in Table IV. The scale is expanded in order to demonstrate the shift between the two "results" for $K\alpha_2^0$ as a consequence of the additional broadening.

IX. DETERMINATION OF $K\alpha_1^0$ AND $K\alpha_2^0$ UNCERTAINTIES

The earlier analysis provides the energies of all components and their uncertainties for all elements of interest. The uncertainties of $K\alpha_1^0$ and $K\alpha_2^0$, depending on the uncertainties of peak height, energies and width of the six fitting components, can be summarized by Eq. (8), where f is a function of 19 parameters giving the positions of $K\alpha_{1,2}^0$, and p_j is the jth parameter

$$\sigma_{K\alpha_{1,2}}^2 < \sum_j \left[\frac{f(p_1,p_2,\ldots,p_j+\sigma_{p_j},\ldots,p_{19}) - f(p_j-\sigma_{p_j})}{2} \right]^2. \tag{8}$$

Most of the parameter uncertainties do not significantly affect the peak positions. From such an investigation, the uncertainty of $K\alpha_1^0$ and $K\alpha_2^0$ energies are shown to be dominated by the uncertainty of centroids of $K\alpha_{11}$ and $K\alpha_{21}$ components, respectively. Other components typically contribute no more than 1% of the overall uncertainty in the peak locations. This is the justification in the earlier literature for the uncertainties in the references for the peak locations being given by the quadrature sum of the $K\alpha_{11}$ or $K\alpha_{21}$ component uncertainties, combined with the absolute determination of the energy scale from the calibration of the spectrometer. The results for vanadium in Tables I and II include uncertainties due to correlations between parameters and hence are robust for the component determination, but overestimate the impact on the determination of the peak. A constrained fit of the same data yields the actual uncertainty of the peak determination as given in Table IV. This latter estimate is fully consistent with the estimated peak uncertainty of $\sigma = \mathrm{FWHM}/\sqrt{N}$ where N is the number of counts collected in the peak. This prescription yields consistent results (in fact, the literature results) for all peak uncertainties for these $K\alpha$ profiles.

X. DISCUSSION: COMPONENT AND PEAK DETERMINATIONS FOR VANADIUM

The determination of all component parameters and uncertainties is given in Tables I and II, and the determination of the scale of the data in our vanadium spectrum is dominated by the uncertainty of the reference calibration, but has additional minor contributions from the peak shift due to the change of resolution and due to our statistical determination of the peak of our raw experimental data. Of course, the last uncertainty can be reduced with additional spectra and statistics, whereas the resolution dependent uncertainty is somewhat fixed but quite small.

The component uncertainties for the $K\alpha_{12}$, $K\alpha_{13}$, and $K\alpha_{22}$ centroids are relatively poor for this vanadium profile determination, as was also true for the original and remodeled results of the other elements. The fitted values tabulated were the result of a completely free fit of all parameters, with a variety of independent initial parameters. The solution was robust.

However the matrix was singular, because of correlations between components and derivative signatures. Tabulated

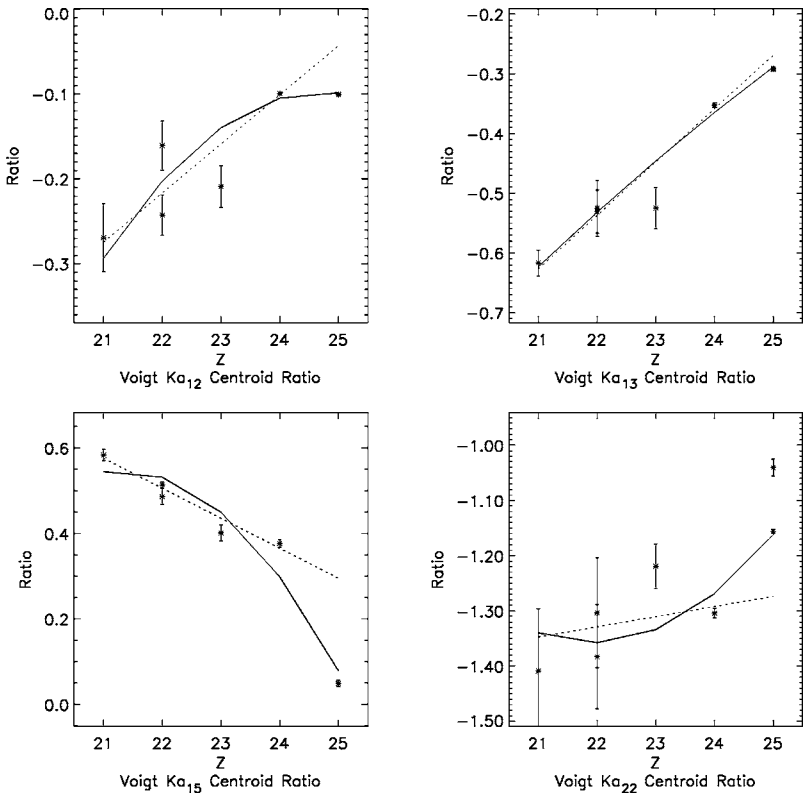

FIG. 15. Voigt $R_{\alpha_{jk}}$ centroid coefficient ratios, as obtained in the present results.

uncertainties were found by constraining 2 or 4 parameters (see tables) to the determined values and refitting. This is a singular value decomposition approach, but with an iterative method and allowing specific physical parameters to be isolated separately. Accordingly, uncertainties of the remaining parameters were determined by separate fits where the singular values were removed by constraining other parameters. The literature sources have implicitly used a similar approach by fixing the Gaussian width prior to the fitting of the remaining parameters. There were no width anomalies in this result, so that natural physical meaning may be assigned.

The method for fitting used in Ref. [15] is also a Levenberg-Marquardt method, but that the parameter errors and fits are determined by an iterative sequential "single" parameter fit. We have included much more of the estimates of correlated uncertainty in the tabulated results for vanadium, and hence have provided uncertainties which may, by contrast, be robust overestimates of precision. However, we agree with those authors on the relevant error corresponding to the peak location definition.

XI. DISCUSSION: CONSISTENCY AND TRENDS FOR THE EXPERIMENTAL SERIES

What is the consistent structure in the satellite components to the diagram lines of the spectrum? Do they show a reliable trend with atomic number, and hence may these be useful physical representations of real structure, and structure evolution with atomic number?

The same coefficients discussed in Sec. VI may be used to consider these questions based on the experimental results and uncertainties. The results for the Voigt profile analysis are plotted in Figs. 15–17, and general trends are clear.

The results for the two separate titanium data sets are distinct, especially for the $R_{\alpha_{12}}$ centroid coefficient ratio, but even for this parameter the results are only about two standard deviations discrepant. Some simple limits may be observed by inspection of the data: the ratio for $K\alpha_{22}$ must always be less than -1 (i.e., on the left of the $K\alpha_{21}$ diagram line which determines the scale); that for $K\alpha_{15}$ must always be greater than 0 (i.e., on the right of the $K\alpha_{11}$ diagram line which determines the scale); and the other two components fitted must lie between the two diagram lines and hence with centroid coefficient ratios between 0 and -1. Given this, there is a clear result that the $K\alpha_{12}$, $K\alpha_{13}$, and $K\alpha_{22}$ centroids are shifting towards the strongest $K\alpha_{11}$ peak with increasing atomic number over this range.

Some kind of anomaly can be seen for manganese, suggesting a nonsmooth development of structure for the highest $Z=25$. Accordingly, two fits of the trends have been made. The first is a simple linear trend from $Z=21$ to $Z=24$, extrapolated to $Z=25$ for completeness. All of the points below $Z=25$, including the current results for vanadium, lie within two standard deviations of this trend, implying a possible very simple interpretation of the evolution of structure.

The other plot is also a simple quadratic interpretation, and primarily indicates the departure from the earlier trend of the manganese spectrum. Accordingly, this quadratic fit includes the manganese parameter components in its fit, as tabulated in Table I.

From Table II of Ref. [15], we have used the relative integrated intensities to reconstruct the profile, prior to remodeling the data. This is inconsistent with the tabulated relative amplitude coefficient for the $K\alpha_{22}$ component from

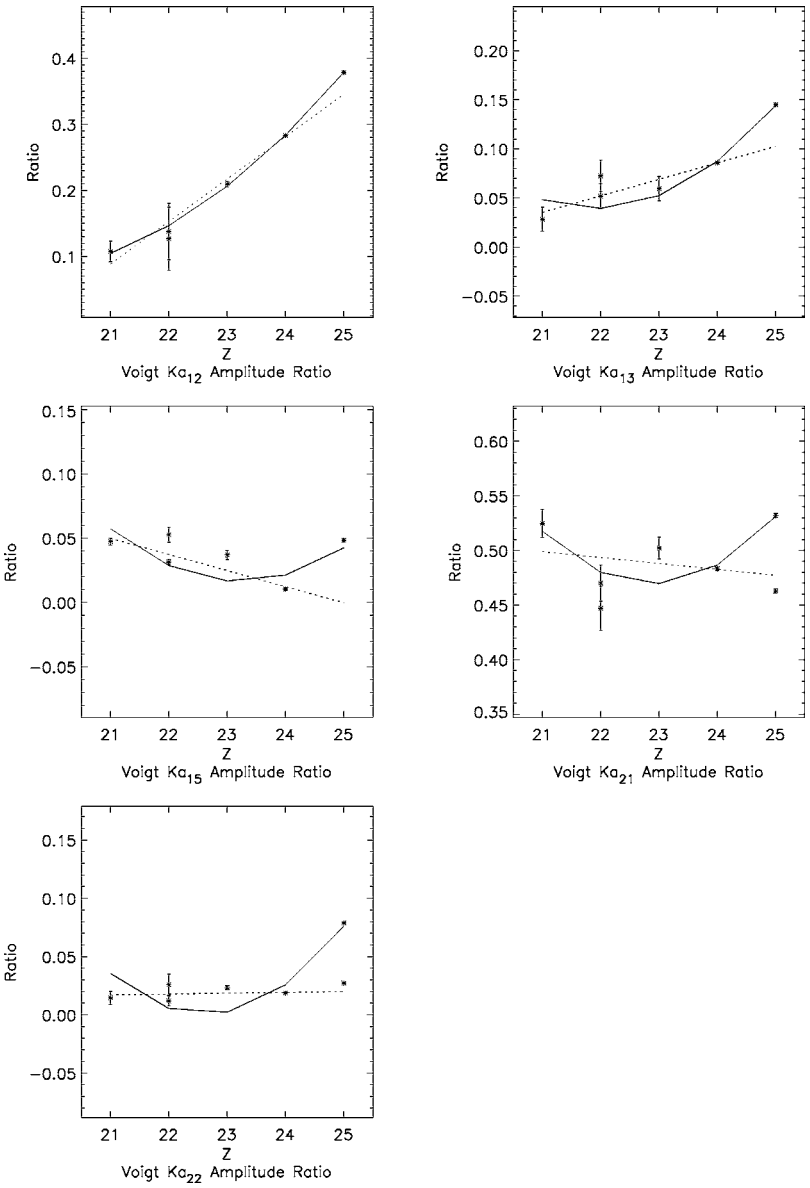

FIG. 16. $A_{\alpha_{jk}}/A_{\alpha_{11}}$ amplitude ratios. The coefficients display a smooth and reliable trend.

the same table. There is a typographical error in one of these numbers, by a factor of ten (i.e., one "0"). We have modeled both alternatives, and conclude that both [15,24] have used and assumed the relative intensity ratio for $K\alpha_{22}$ given in that table in their further analysis. Hence we follow this conclusion in our tabulation and in the fitting of the quadratic trend. However, we include the results from a full modeling of the other alternative as the second "manganese" point ($Z=25$) on the plots of the coefficients. For most parameters this confusion does not affect conclusions regarding trends or strutcture. For the $K\alpha_{22}$ component it obviously has a significant quantitative effect, but the qualitative conclusion—that a structural change is emerging with manganese—is unaffected by this choice.

The results for the amplitude coefficient ratios are smooth and stable within uncertainty, and hence are quite robust. Several of the widths of the weaker or correlated components display more scatter or noise than a clear trend, but they do generally display a consistency. The best determined width, the Lorentzian width as a fraction of the $C_{\alpha_{11}}-C_{\alpha_{21}}$ separation, is a very strong and clear trend, as given in Fig. 17. The strongest deviation from these trends are an increase in the width of $K\alpha_{21}$ for vanadium and a corresponding narrowing of the vanadium width for the adjacent peak $K\alpha_{13}$. As a trend, this is clearly an inconsistency, but for one relatively minor parameter out of 19.

The corresponding ratios for LS fitting may be fully reconstructed from the tabulated data. The elements other than vanadium are consistent between the two profile approaches, as discussed above; and the vanadium parameters from the LS fitting are significantly more discrepant than from the Voigt fitting. Hence we would argue that Voigt fitting is often essential for broadened spectra and is sufficient for most spectra. This may be compared, for example, to a detailed prediction of shape and profile based on diffraction theory with all parameters well defined and known. The choice of component profile shape does not significantly affect the determination of the peak location, or significant details of the profile determination, above about a 1 ppm (part per million) level.

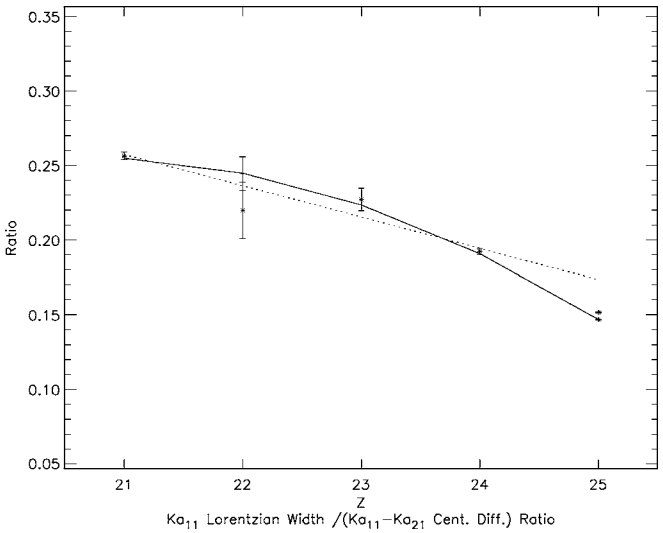

FIG. 17. $L_{\alpha_{11}}/C_{\alpha_{11}}-C_{\alpha_{21}}$ ratio of the Lorentzian width of the dominant component compared to the scale given by the separation in energy of the diagram lines. A smooth and reliable trend is clear.

XII. CONCLUSIONS

There are very strong trends in the development of the satellite and profile structure of $K\alpha$ with atomic number which have been characterized in this study. Some authors have defined a general "asymmetry parameter" to characterize structure of a particular spectral line. That approach quite neglects the variation of the location and amplitude of specific physical satellite contributions. Reference [15] argues this very well, specifically that "the simplified approach of addressing only the width and asymmetry of a line is insufficient to account for the shapes of complex spectra such as those of the 3*d* transition metals."

There has been some other investigation of dominant contributions from 1*s*-2*p* and 1*s*3*d*-2*p*3*d* transitions. Dirac-Fock *ab initio* calculations have certainly confirmed key details of the profile structure, and concluded that structural complexity is likely to reach a peak with a maximum number of open shells (i.e., with Fe, $Z=26$). The key study looked at $Z=24$ through $Z=29$ [15] and concluded that the structural changes around Mn and Fe were quite significant. Our study from $Z=21$ to $Z=25$ addresses the neighboring region and concludes that evolution of structure from Sc through Cr is remarkably smooth and uniform but, irrespective of some model assumptions, that there is a discontinuity in this evolution when Mn is reached, probably because of the increasing number of open *d* shell electrons. At this point an isolated atomic and a (metallic) solid electron configuration in the ground state or in the hole state are not at all identical, and this calibration study investigates (metallic) solid targets of high purity, bombarded with electrons with energies much higher (2–3 times) than the characteristic energy for the inner shell transition. If such conditions are followed, then profiles are expected to be moderately uniform at the level of accuracy determined, and the comparison between results for the two titanium data sets is a useful check on this detail.

$K\alpha$ profiles have been characterized to high accuracy in a form which is suitable for application to lower resolution spectra from single crystal or curved crystal diffraction, for example, without loss of accuracy. The profiles have been separated into six peaks, and an overall Gaussian width is recommended for much additional broadening; with individual Lorentzian widths for each component as described and tabulated above. This has involved detailed reanalysis of Sc, Cr, and Mn data; analysis of two sets of Ti data; and experimental data for vanadium, which has served to both confirm the structural trends suggested from the other data and to yield a robust and defined method for the tertiary transfer of accurate standards at the level of a few parts per million.

ACKNOWLEDGMENTS

This research has involved discussions with G. Christodoulou and P. Indelicato which are gratefully acknowledged. We also acknowledge raw data from J. Kawai. We acknowledge all the experimental team from the NIST EBIT, including Larry Hudson, John Gillaspy, Albert Henins, Joshua Pomeroy, and Joseph Tan; and an ARC grant which has permitted this research.

[1] R. D. Deslattes and A. Henins, Phys. Rev. Lett. **31**, 972 (1973).
[2] P. Becker, P. Seyfried, and H. Siegert, Z. Phys. B: Condens. Matter **48**, 17 (1982).
[3] R. D. Deslattes, M. Tanaka, G. L. Greene, A. Henins, and E. G. Kessler, Jr., IEEE Trans. Instrum. Meas. **IM-36**, 166 (1987).
[4] G. Basile, A. Bergamin, G. Cavagnero, G. Mana, E. Vittone, and G. Zosi, Phys. Rev. Lett. **72**, 3133 (1994).
[5] K. Nakayama and H. Fujimoto, IEEE Trans. Instrum. Meas. **46**, 580 (1997).
[6] E. G. Kessler, A. Henins, R. D. Deslattes, L. Nielsen, and M. Arif, J. Res. Natl. Inst. Stand. Technol. **99**, 1–18 (1994).
[7] E. G. Kessler Jr., J. E. Schweppe, and R. D. Deslattes, IEEE Trans. Instrum. Meas. **46**, 551–555 (1997).
[8] R. D. Deslattes, E. G. Kessler Jr., P. Indelicato, L. de Billy, E. Lindroth, and J. Anton, Rev. Mod. Phys. **75**, 35–99 (2003).
[9] B. L. Scott, Phys. Rev. A **34**, 4438–4441 (1986).
[10] S. Doniach and M. Sunjic, J. Phys. C **3**, 285–291 (1970).
[11] D. F. Anagnostopoulos, R. Sharon, D. Gotta, and M. Deutsch, Phys. Rev. A **60**, 2018 (1999).
[12] M. Deutsch, G. Holzer, J. Hartwig, J. Wolf, M. Fritsch, and E. Forster, Phys. Rev. A **51**, 283 (1995).
[13] M. Deutsch (private communication).
[14] D. F. Anagnostopoulos, D. Gotta, P. Indelicato, and L. M. Simons, Phys. Rev. Lett. **91**, 240801 (2003).
[15] G. Holzer, M. Fritsch, M. Deutsch, J. Hartwig, and E. Forster, Phys. Rev. A **56**, 4554 (1997).

[16] N. Shigeoka, H. Oohashi, T. Tochio, Y. Ito, T. Mukoyama, A. M. Vlaicu, and S. Fukushima, Phys. Rev. A **69**, 052505 (2004).
[17] J. A. Bearden, Rev. Mod. Phys. **39**, 78 (1967).
[18] Y. Cauchois and C. Senemaud, *Tables Internationales De Constantes Selectionnees. 18. Longeurs d'onde des emissions X et des discontinuites d'absorption X* (Pergamon Press, London, 1978).
[19] J. A. Bearden, A. Henins, J. G. Marzolf, W. C. Sauder, and J. S. Thomsen, Phys. Rev. A **135**, 899 (1964).
[20] J. Kawai, E. Nakamura, Y. Nihei, K. Fujisawa, and Y. Gohshi, Spectrochim. Acta, Part B **45B**, 463–479 (1990).
[21] J. Kawai, T. Konishi, A. Shimohara, and Y. Gohshi, Spectrochim. Acta, Part B **49B**, 725–738 (1994).
[22] J. D. Gillaspy, Phys. Scr. **65**, 168 (1996). J. D. Gillaspy (private communication).
[23] M. K. Kinnane, J. A. Kimpton, M. D. de Jonge, K. Makonyi, C. T. Chantler, Meas. Sci. Technol. (unpublished).
[24] R. D. Deslattes, E. G. Kessler Jr., and P. Indelicato, *et al.*, Rev. Mod. Phys. **75**, 35–99 (2003).